RSC Advances

ROYAL SOCIETY OF CHEMISTRY

www.rsc.org/advances

Graphical and textual abstract

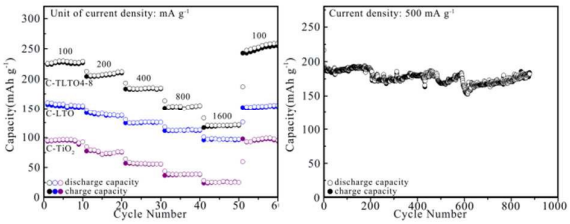

Carbon-coated $TiO_2/Li_4Ti_5O_{12}$ composite with Li:Ti=4:8 displays high rate capacities and excellent long-term cycling performance at high current density.

Journal Name

ARTICLE

Excellent performance of carbon-coated $TiO_2/Li_4Ti_5O_{12}$ composite with low Li/Ti ratio for Li-ion storage

Received 00th January 20xx,
Accepted 00th January 20xx

DOI: 10.1039/x0xx00000x

www.rsc.org/

Wei Yang, Xue Bai, Tao Li, Yuan-Yuan Ma, Yong-Xin Qi, Long-Wei Yin, Hui Li, Ning Lun*, Yu-Jun Bai*

$TiO_2/Li_4Ti_5O_{12}$ composites with different Li:Ti molar ratios were fabricated by simply hydrolyzing tetrabutyl titanate in the water solution of $LiNO_3$ and calcining the dried mixture at 600 °C, and the carbon-coated composites were prepared at 600 °C employing glucose as carbon precursor. Compared to the carbon-coated TiO_2 and $Li_4Ti_5O_{12}$ prepared under the similar conditions, the carbon-coated $TiO_2/Li_4Ti_5O_{12}$ composite with Li:Ti=4:8 exhibits a stable capacity of 227.2 mAh g^{-1} when cycled 100 times at a current density of 100 mA g^{-1}, and when cycled at 200, 400, 800 and 1600 mA g^{-1}, the corresponding capacities are 206.1, 183.0, 152.4 and 119.4 mAh g^{-1} with the Coulombic efficiency close to 100%. The composite also reveals outstanding long-term cycling stability at 500 mA g^{-1} with a reversible capacity of 177.6 mAh g^{-1} after 850 cycles. The enhanced electrochemical performance is ascribed to the synergistic effect of the two phases of TiO_2 and $Li_4Ti_5O_{12}$ with the carbon coating.

1. Introduction

Ti-based compounds, such as TiO_2 and $Li_4Ti_5O_{12}$ (LTO), have demonstrated to be applicable for Li-ion batteries (LIBs) as anode materials with high-power density due to their cycling stability, outstanding capacity retention and high Coulombic efficiency during charging-discharging at varied current rates [1].

LTO with a spinel structure exhibits some unique superiorities, such as zero structure change during charge-discharge process, long plateau at 1.55 V (vs Li^+/Li) and improved safety resulted from the high operating potential [2], thus revealing remarkable cycling stability and rate capabilities. However, the disadvantages of poor electronic and ionic conductivities, low theoretical capacity (175 mAh g^{-1}), as well as high cost owing to the high Li content with limited resource restrict the wide application of LTO in high-rate LIBs.

TiO_2 possesses some polymorphs such as anatase TiO_2 (A-TiO_2), rutile TiO_2 (R-TiO_2), brookite TiO_2 and TiO_2-B, whose electrochemical performance varies with the structure, morphology, size and preparation method [3]. In comparison with the R-TiO_2, Li^+ storage in the A-TiO_2 is more readily due to the open channel structure [4-6], resulting in a reversible capacity of 167 mAh g^{-1} around the potential plateau of 1.7 V (vs Li^+/Li) [7, 8]. Despite the low cost and simple preparation compared to LTO, the poor electronic and ionic conductivities also limit the applications of A-TiO_2.

Several approaches have been adopted to enhance the electrochemical performance of LTO and TiO_2, including coating carbon [9-12], tailoring morphology [13-15], compositing with other oxides or graphene [16, 17], refining particle size to nanoscale and doping cations or anions [18]. Compositing TiO_2 with LTO (TLTO) is another route that has attracted increasing attention recently. Carbon-coated TLTO (C-TLTO) synthesized by molten salt process exhibited a capacity of 110 mAh g^{-1} at 10 C[19, 20]. LTO nanosheets and nanorods with TiO_2 nanocoating demonstrated enhanced capacity and rate capabilities [21, 22]. TLTO nanocomposite fabricated via hydrothermal route with adding thiourea revealed a capacity of 132 mAh g^{-1} at 1600 mA g^{-1} [23]. Spherical flower-like TLTO prepared by boiling followed by solid-state sintering delivered capacities of 177.2 and 112.5 mAh g^{-1} at 0.5 C and 20 C, respectively [24]. TiO_2 nanotubes composited with nanocrystalline LTO produced by hydrothermal reaction showed outstanding cycling performance and high-rate capability with the mass ratios of 2:8 and 4:6 [25]. C-TLTO powders prepared via solvothermal route displayed a capacity of 140 mAh g^{-1} when cycled 100 times at 5 C [26]. LTO-TiO_2-carbon nanofiber obtained through complex treatment presented capacities of 203.8 and 114.3 mAh g^{-1} corresponding to 100 and 2000 mA g^{-1} [27]. Carbon-decorated LTO/R-TiO_2 mesoporous microspheres synthesized by hydrothermal method followed by calcinating exhibited a capacity of 153.0 mAh g^{-1} at 0.5C [28]. Generally, the electrochemical performance of TLTO and C-TLTO depends greatly on the synthesis temperature and Li/Ti molar ratio. Higher temperature contributes to the formation of LTO in the TLTO [19]. However, the effect of the Li/Ti ratio is complex. The TLTO or C-TLTO with high Li/Ti molar ratio could only improve the capacity slightly due to the small amount of TiO_2 [19-22, 24-28], whereas the TLTO with low Li:Ti molar ratio (1:4 or less) usually consist of more R-TiO_2 rather than A-TiO_2 when the synthesis temperature is above 600 °C [23], resulting in low reversible capacity. Thus the C-TLTO with an

Key Laboratory for Liquid–Solid Structural Evolution and Processing of Materials (Ministry of Education), Shandong University, Jinan 250061, People's Republic of China. E-mail address: lunning66@sdu.edu.cn (N. Lun), byj97@126.com (Y.-J. Bai); Tel/Fax: +86 531 88392315..

Electronic Supplementary Information (ESI) available: [details of any supplementary information available should be included here]. See DOI: 10.1039/x0xx00000x

appropriate Li:Ti ratio might exhibit remarkable performance. However, few systematic investigations are available to date.

In this work we prepared TLTO with different Li/Ti ratios by simply hydrolyzing tetrabutyl titanate (TBT) in the water solution of $LiNO_3$, and the carbon-coated TLTO with Li:Ti=4:8 achieved excellent performance.

2. Experimental Section

2.1. Fabrication of carbon-coated products

The synthesis of C-TLTO with the Li:Ti molar ratio of 4:8 (C-TLTO4-8) is as follows. The solution of 40.84 g TBT dissolved in ethanol was slowly titrated into the solution of 4.137 g $LiNO_3$ dissolved in 10 mL deionized water under magnetic stirring. The mixture was thoroughly dried at 105 °C for 12 h and sintered at 600 °C for 5 h in an electric furnace in air to obtain TLTO4-8. Then 1.5 g of the composite was mixed with 1.05 g glucose in deionized water. The mixture thoroughly dried at 105 °C was put into a stainless steel autoclave, and the sealed autoclave was heated at 600 °C for 5 h to realize fast carbon coating.

The fabrication of C-TLTOs with the Li/Ti molar ratio of 4:7 (C-TLTO4-7) and 4:9 (C-TLTO4-9), carbon-coated TiO_2 (C-TiO_2) and carbon-coated LTO (C-LTO) is simlar to that for C-TLTO4-8.

2.2. Material Characterization

The Ni filtered Cu K_α radiation was used to acquire X-ray diffraction (XRD) patterns of the products at 4° min^{-1} by a Rigaku Dmax-2500 diffractometer (V =50 kV, I =100 mA). Raman spectra were measured by a Lab-RAM HR800 utilizing excitation from an argon ion laser (632.81 nm in wavelength). The morphology was examined by a JEOL JEM-2100 high-resolution transmission electron microscope (HRTEM). And thermogravimetric (TG) curves were evaluated using a SDT-Q600 V8.3 Build 101 at a heating rate of 10.0 °C min^{-1} from ambient temperature to 800 °C in air.

2.3. Electrochemical measurement

The electrochemical performance was evaluated by assembling 2025 coin-type cells. The uniform slurry containing active materials, polyvinylidene fluoride (dissolved in n-methyl pyrrolidinone), and carbon black with a weight ratio of 8:1:1 was pasted on a copper foil substrate and thoroughly dried at 120 °C for 12 h in a vacuum oven. Pure lithium foil was used as the counter electrode and Celgard 2300 as separator. A mixture of 1 M $LiPF_6$ in dimethyl carbonate and ethylene carbonate (with a volume ratio of 1:1) was utilized as electrolyte. The half-cells were assembled at ambient temperature in a glove box full of argon. Galvanostatic discharge/charge was performed in a potential range of 0.02-3 V (vs Li^+/Li) at different current densities. The mass of active materials on each electrode (14 mm in diameter) is 3.0 mg or so.

An IviumStat electrochemistry workstation was employed to measure cyclic voltammograms (CV) in the potential range of 0.01-3 V (vs Li/Li^+) at different scan rates and electrochemical impedance (EI) spectra with an AC signal amplitude of 10 mV with the frequency range from 100 kHz to 0.01 Hz.

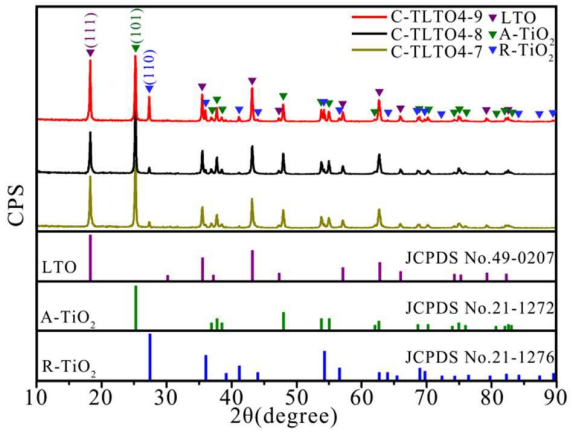

Fig. 1 XRD patterns of C-TLTO4-7, C-TLTO4-8 and C-TLTO4-9.

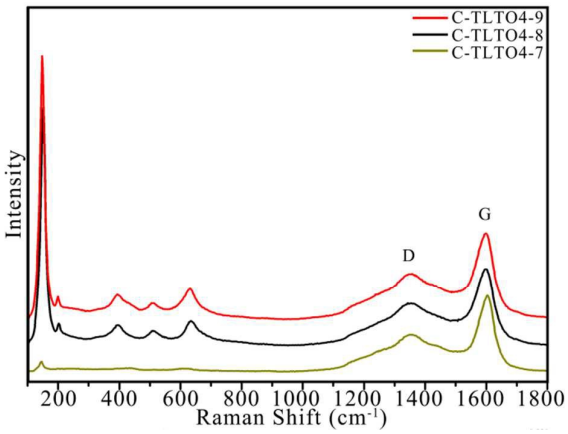

Fig. 2 Raman spectra of C-TLTO4-7, C-TLTO4-8 and C-TLTO4-9.

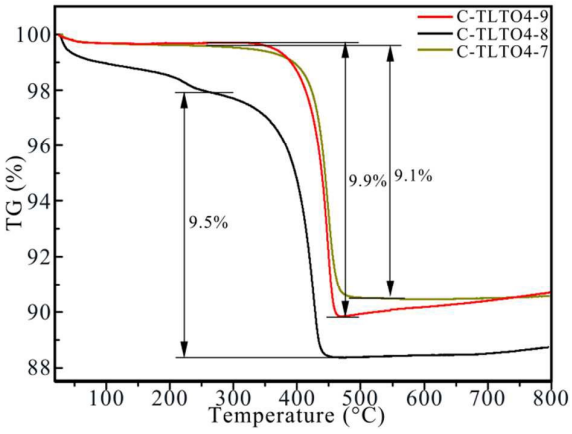

Fig. 3 TG curves of C-TLTO4-7, C-TLTO4-8, C-TLTO4-9.

3. Results and Discussion

3.1. Structure and morphology of the carbon-coated products

The XRD patterns of the carbon-coated products are shown in **Fig. 1**. The products are comprised of LTO, A- and R-TiO_2, and the content of R-TiO_2 increases with decreasing the Li/Ti molar ratio. The average crystallite size calculated by Scherrer formula ($D = K\lambda/B\cos\theta$) is about 40.0 nm for LTO, A- and R-TiO_2 in the products owing to the same sintering temperature of 600 °C.

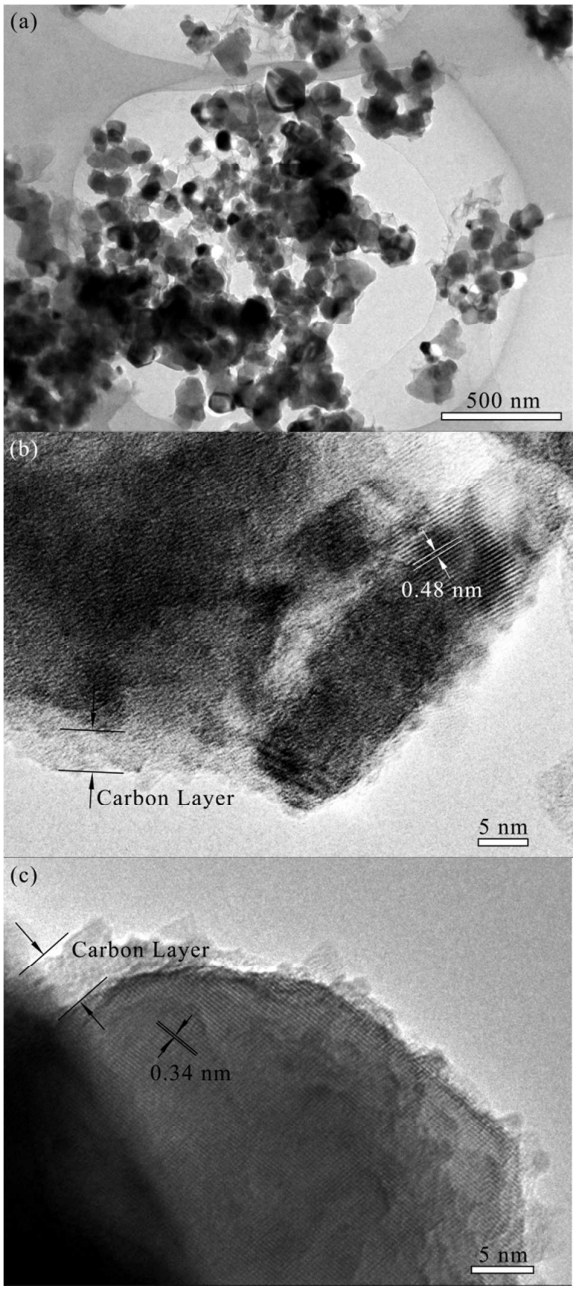

Fig. 4 TEM images of C-TLTO4-8.

The carbon structure in carbon-coated products was evaluated by Raman spectrum, as shown in **Fig. 2**. The five vibration peaks around 151, 202, 393, 507 and 634 cm^{-1} match well with those from A-TiO_2 ($A_{1g}+2B_{1g}+3E_g$) [29], and their peak intensities decrease with increasing the Li/Ti molar ratio, consistent with the XRD results. Another two peaks around 1345 and 1597 cm^{-1} are resulted from the disordered carbon (D-band) and graphitic carbon (G-band) [30, 31], and the intensity ratio of the two bands (I_D/I_G) indicates the graphitization degree [32]. The absence of LTO peaks in C-TLTOs is due to its weak Raman scattering activity. From the I_D/I_G value of 1.8 calculated, the carbon in the C-TLTO4-8 is in amorphous state. The Raman spectra of other carbon-coated products are similar to that of C-TLTO4-8 owing to the identical carbonization temperature of 600 °C using the same carbon source of glucose.

The carbon content was determined by TG analysis. From the TG curve of C-TLTO4-8 in **Fig. 3**, the slight weight loss of 2.1% below 275 °C results from the desorption of water absorbed on the product, and the main loss of 9.5% in the range of 275-475 °C from the oxidation of carbon, i.e. the carbon content in C-TLTO4-8 is 9.5 wt%, and that in C-TLTO4-7 and C-TLTO4-9 is 9.1 and 9.9 wt%, respectively.

The structure and morphology of C-TLTO4-8 was characterized by TEM, as shown in **Fig. 4**. From the low magnification image in **Fig. 4a**, the particles range from 30 to 50 nm in diameter, consistent with the XRD result. From the high resolution images in **Figs. 4b** and **4c**, the d-spacing of 0.48 nm could be indexed to that of (111) plane of spinel LTO and 0.34 nm to that of (101) plane of the A-TiO_2, further confirming the formation of composite of LTO and TiO_2. The carbon layer on the nanoparticles is from 2 to 6 nm in thickness. The morphology of other carbon-coated products is analogous to that of C-TLTO4-8.

3.2. Electrochemical performance

Cycling performance was tested at 100 mA g^{-1} adopting at least five cells for every product, as shown in **Fig. 5**. From **Fig. 5a**, the low Coulombic efficiency in the 1st cycle results from the formation of solid electrolyte interphase (SEI) on the carbon coating [33], resulting in the capacity decrease from 398.2 to 195.1 mAh g^{-1} for C-TLTO4-8. After cycling 100 times, the reversible capacity for C-TLTO4-8 is 227.2 mAh g^{-1}, which greatly exceeds the theoretical capacity of LTO owing to the compositing with A-TiO_2 and the carbon coating, and is also prior to those for C-TLTO4-7 (201.1 mAh g^{-1}) and C-TLTO4-9 (83.6 mAh g^{-1}). The change in capacity is associated with the variation of R-TiO_2 in the composite, because the grain size and morphology of the constituents are similar. Although the theoretical capacity of the composite increases with decreasing the Li:Ti ratio, excessive R-TiO_2 in the composite could result in adverse effect on the lithium storage, suggesting that the electrochemical performance associates significantly with the Li:Ti molar ratio in the TLTO composite.

As a comparison, the cycling performance of C-LTO and C-TiO_2 prepared under the similar conditions was also tested at 100 mA g^{-1} (**Fig. 5b**). Apparently, the reversible capacity of C-TLTO4-8 after cycling 100 times is markedly higher than those of C-LTO (162.9 mAh g^{-1}) and C-TiO_2 (122.6 mAh g^{-1}), demonstrating the synergistic effect resulted from the composite of the two phases of TiO_2 and

LTO. It seems that the lithium storage in the TLTO composite is easier than in individual phases, because the grain boundaries between TiO_2 and LTO nanoparticles provide abundant sites for Li^+ storage[20], contributing to achieving high capacity. Also, besides acting as a physical barrier to protect the active materials[32] , the carbon coating could participate in the electrochemical reaction and create interface for additional interfacial lithium storage according to our supporting information.

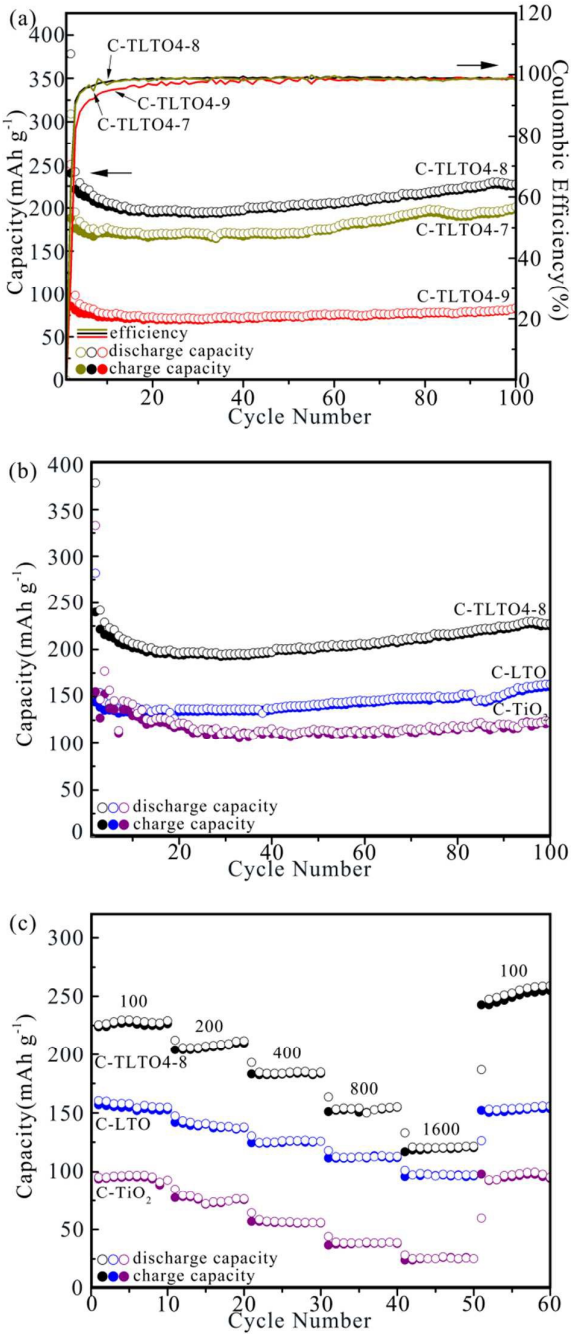

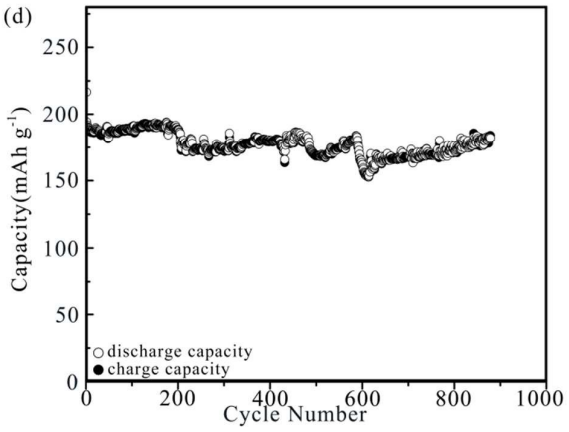

Fig. 5 Cycling performance at 100 mA g^{-1} for C-TLTO4-7, C-TLTO4-8 and C-TLTO4-9 **(a)**, and C-TLTO4-8, C-LTO, and C-TiO_2 **(b)**, rate performance for C-TLTO4-8, C-LTO, and C-TiO_2 **(c)**, and long-term cycling performance of C-TLTO4-8 at 500 mA g^{-1} after the rate performance test **(d)**.

Tab. 1 Reversible capacitities (mAh g^{-1}) at varied current densities (mA g^{-1}) for the carbon-coated products.

Sample	Capacities at varied densities					
	100	200	400	800	1600	100
C-TLTO4-8	228.1	208.0	184.2	153.4	120.9	254.1
C-LTO	156.9	139.6	125.8	112.7	97.4	154.2
C-TiO_2	95.4	75.9	56.6	38.7	25.6	96.8

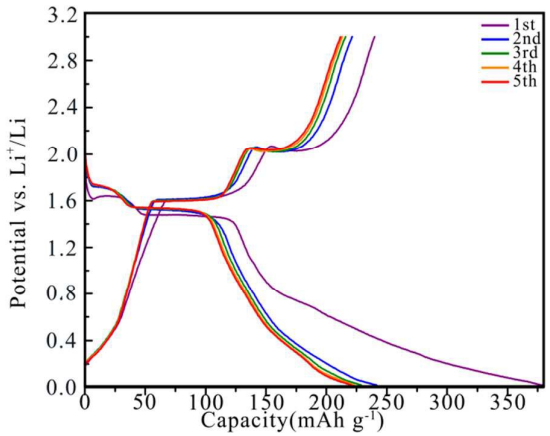

Fig. 6 Charge-discharge curves of C-TLTO4-8 for the first five cycles at 100 mA g^{-1}.

The rate performance of C-TLTO4-8, C-LTO and C-TiO_2 was measured after cycling 100 times at 100 mA g^{-1}, as shown in **Fig. 5c**. Obviously, the capacities of C-TLTO4-8 are higher than those of C-LTO and C-TiO_2 at the corresponding densities. The detailed capacities are summarized in **Tab. 1**. The plentiful interfaces in the composites provide the possibility to additionally store Li-ions and produce extra capacity, so the high capacity could be partially attributed to this fast faradaic pseudocapacitive Li storage.[23] Also the interfaces formed by irregularly arranged atoms could act as channels for ease Li-ion traverse through, accelerating the Li-ion insertion and extraction process, so the composites achieve excellent rate performance.

When the current density is restored to 100 mA g^{-1}, a capacity of 254.1 mAh g^{-1} was retained for C-TLTO4-8, increased by 11.4% compared to that after the initial 100 cycles. The increase in capacity with cycling also occurs in other anode materials, which could be explained as the activation effect due to the synergistic combination of the two phases of TiO_2 and LTO, as well as the optimization of stable SEI [34].

Long-term cycling performance for C-TLTO4-8 was tested at 500 mA g^{-1} immediately after the rate performance measurement, as displayed in **Fig. 5d**. When cycled 850 times, a reversible capacity 177.6 mAh g^{-1} is nearly stably retained, indicative of the excellent long-term cycling stability even at the high current density of 500 mA g^{-1}.

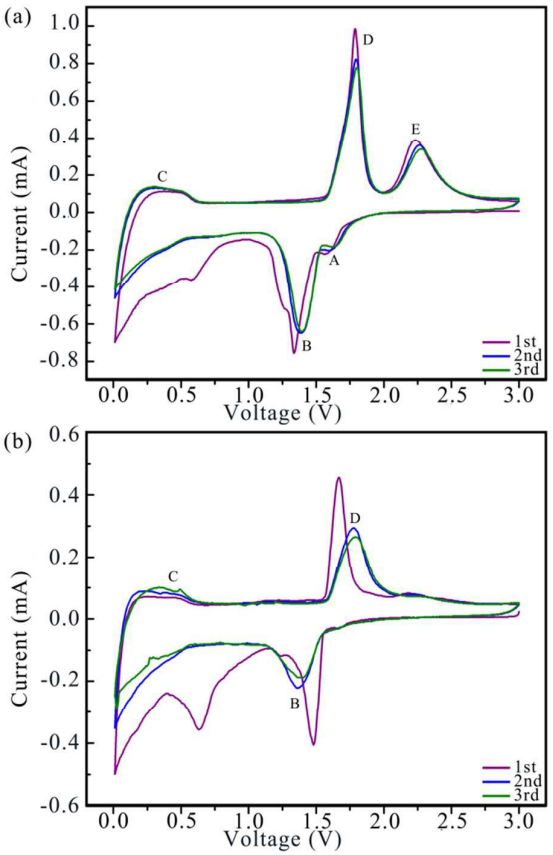

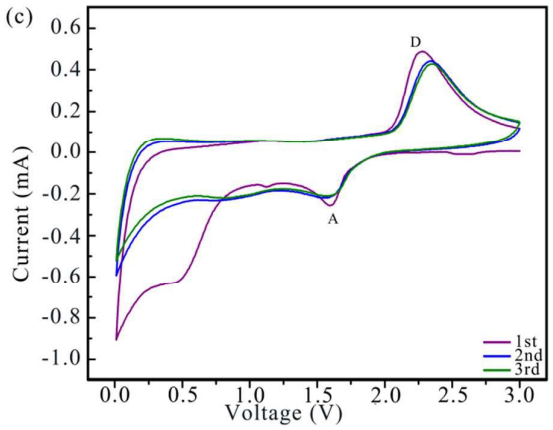

Fig. 7 CV plots of C-TLTO4-8 **(a)**, C-LTO **(b)** and C-TiO_2 **(c)** at the scan rate of 0.3 mV s^{-1} between 0.01 and 3.0 V for the initial three cycles.

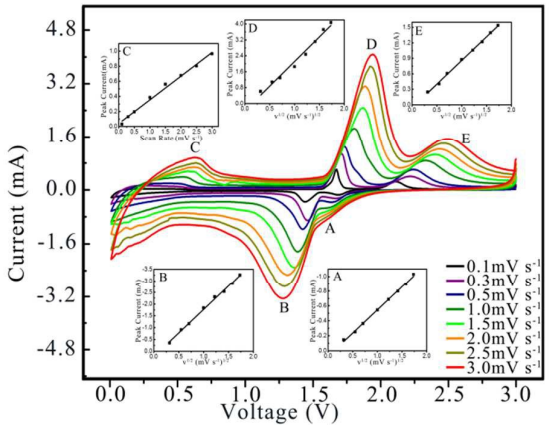

Fig. 8 CV plots of C-TLTO4-8 at different scan rates between 0.01 and 3.0 V after the initial three cycles. The inserts display the relationship between the peak current and scan rate.

To further understand the reactions occurred during charging-discharging of C-TLTO4-8, voltage-capacity profiles at 100 mA g^{-1} are provided in **Fig. 6a**. During discharging, two plateaus around 1.8 and 1.4 V correspond to the lithiation of A-TiO_2 and LTO, respectively, whereas during charging, the two plateaus around 2.0 and 1.6 V to the delithiation of the two phases, further indicating the formation of TiO_2 and LTO composite. Both the charge and discharge curves are nearly superposed after the 1st cycle, demonstrative of the excellent cycling stability of C-TLTO4-8. From the 2nd cycle, the potential difference between the cathodic and anodic plateaus becomes small compared to that in the 1st cycle, demonstrating the activation effect and decreased polarization due to the faradaic pseudocapacitive Li-ion storage in the composite of TiO_2 and LTO.

The electrochemical reactions were further investigated by CV plots (**Fig. 7**). The reduction peak around 0.6 V in the 1st cycle is ascribed to the formation of SEI on the carbon layer [35], which fades away in the following cycles. From the 2nd cycle, the curves almost coincide with each other. From **Fig. 7a**, C-TLTO4-8 exhibits two distinct pairs of redox peak around 1.80/1.39 V and 2.28/1.56 V.

Associated with the CV plots for C-LTO (**Fig. 7b**) and C-TiO_2 (**Fig. 7c**), the pair of 1.39/1.56 V (peaks B and D) corresponds to the Li^+ insertion/deinsertion in the spinel LTO [36-38], and the one of 1.8/2.28V (peaks A and E) to that in A-TiO_2 phase [39-41]. The oxidation peak below 0.6 V (peak C) in **Figs. 7a** and **7b** results from a multi step restore of Ti^{4+} in LTO.[42] A small reduction peak at 1.28 V occurred in the 1st cycle of C-LTO and C-TiO_2 is due to the irreversible phase transformation from the small amount of R-TiO_2 to Li_xTiO_2 [43, 44]. Note that both C-LTO and C-TiO_2 exhibit obvious polarization after the 1st cycle, whereas C-TLTO4-8 reveals almost no polarization, demonstrating the priority of the composite as anode material for LIBs.

To better account for the enhanced electrochemical performance of C-TLTO4-8, cyclic voltammograms were measured at different scan rates between 0.01 and 3.0 V after the initial three cycles, as shown in **Fig. 8**, and the relationship between the peak current and scan rate is displayed in the inserts. Apparently, the peak currents for A, B, D, E are directly proportional to the square root of scan rate, demonstrating the diffusion-controlled reaction for the Li-ion insertion in or extraction from LTO and A-TiO_2 according to the Randles-Sevcik equation[27]:

$$I_p=2.678\times10^5An^{3/2}C_{Li}D_{Li}^{1/2}v^{1/2}\ (25\ ^\circ C)$$

where I_p refers to the peak current in amps, n to the number of electrons transferred in the redox event, and A to the electrode area (cm^2). C_{Li} and D_{Li} are the concentration in mol/cm^3 and the diffusion coefficient in cm^2/s. v represents the scan rate in V/s.

Although the side peak resulted from pseudocapacitive effect at around 1.2 V in the cathodic process (reported in [23, 27]) could not be clearly detected, the good linear correlation between the peak current of C and the scan rate certainly reveals a surface-confined charge-transfer process.[23, 45]

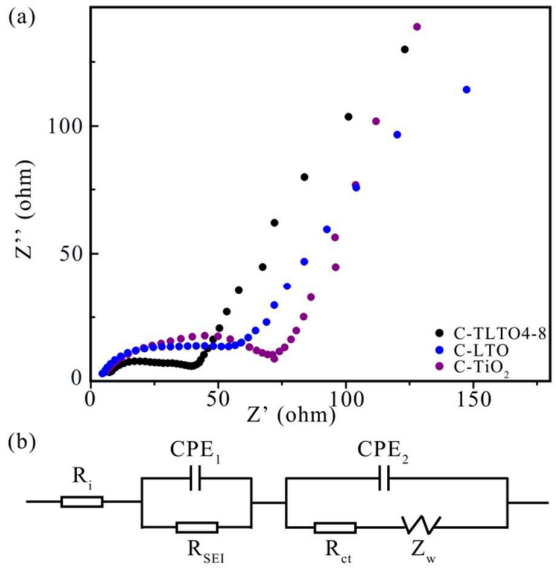

Fig. 9 Impedance spectra of C-TLTO4-8, C-LTO and C-TiO_2 after cycling 60 times at 100 mA g^{-1} **(a)**, and the corresponding equivalent circuit **(b)**.

The electrochemical performance is greatly associated with the EI spectra of cells. The Nyquist plots of C-TLTO4-8, C-LTO and C-TiO_2 after cycling 60 times at 100 mA g^{-1} are displayed in **Fig. 9a**. The curves consist of a depressed semicircle reflecting the electrochemical reaction resistance in high-middle frequency region and an inclined line corresponding to the solid-state diffusion of Li-ion in low frequency region.[46] The corresponding equivalent circuit is provided in **Fig. 9b**, where R_i refers to the uncompensated internal resistance, CPE_1 and CPE_2 to the constant phase elements of the surface layer and double layer, R_{SEI} and R_{ct} to the resistance of SEI and charge transfer process, and Z_w to the Warburg impedance. The R_{ct} for C-TLTO4-8 is 39 Ω, lower than that for C-LTO (53 Ω) and C-TiO_2 (72 Ω), consistent with the electrochemical performance. The enhanced electronic conductivity is possibly associated with the interfacial pseudocapacitive effect at the grain boundaries between LTO and TiO_2 as well as the relatively low surface charge-transfer resistance in the dual phases [23, 27].

Conclusions

In summary, carbon-coated $TiO_2/Li_4Ti_5O_{12}$ composite with the Li:Ti molar ratio of 4:8 fabricated by the simple hydrolysis of tetrabutyl titanate in the water solution of $LiNO_3$ exhibited higher capacity than the carbon-coated TiO_2 and $Li_4Ti_5O_{12}$ prepared under the similar conditions, outstanding rate capabilities and long-term cycling stability at a high current density of 500 mA g^{-1}. The composite could be potentially utilized in LIBs requiring for high power density and high energy density.

Acknowledgements

This work was supported by Shandong Provincial Natural Science Foundation, China (ZR2015EM016), Science and Technology Development Project of Shandong Province (2014GGX102009 and 2015GGX102005), and Independent Innovation Foundation of Shandong University, IIFSDU (2012ZD004).

Notes and references

1. G. N. Zhu, Y. G. Wang and Y. Y. Xia, *Energy Environ. Sci.*, 2012, **5**, 6652.
2. F. X. Wu, X .H. Li, Z. X. Wang, H. J. Guo, L. Wu, X. H. Xiong and X. J. Wang, *Powder Technol.*, 2011, **213**, 192.
3. F. Ning, Y. B. He, B. Li, H. Dua, D. Zhai and F. Kang, *J. Alloys Compd.*, 2012, **513**, 524.
4. D. Wang, D. Choi, Z. Yang, V. V. Viswanathan, Z. Nie, C. Wang, Y. Song, J. G. Zhang and J. Liu, *Chem. Mater.*, 2008, **20**, 3435.
5. G. S. Zakharova, C. Jähne, A. Popa, C. Täschner, T. Gemming, A. Leonhardt, B. Büchner and R. Klingeler, *J. Phys. Chem. C*, 2012, **116**, 8714.
6. J. Li, Z. Tang and Z. Zhang, *Electrochem. Solid-State Lett.*, 2005, **8**, A316.

7. C. H. Sun, X. H. Yang, J. S. Chen, Z. C. H. Sun, X. H. Yang, J. S. Chen, Z. Li, X. W. Lou, C. Z. Li, S. C. Smith, G. Q. Lu and H. G. Yang, *Chem. Commun.*,2010, **46**, 6129.
8. Y. Ren, L. J. Hardwick and P. G. Bruce, *Angew. Chem. Int. Ed.*, 2010, **122**, 2624.
9. J. B. Kim, D. J. Kim, K. Y. Chung, D. Byun and B. W. Cho, *Phys. Scr.* 2010, **T139**, 014026.
10. P. Chang, C. Huang and R. Doong, *Carbon*, 2012, **50**, 4259.
11. S. J. Park, H. Kim, Y. J. Kim and H. Lee, *Electrochim. Acta*, 2011, **56**, 5355.
12. S. J. Park, Y. J. Kim and H. Lee, J. Power Sources, 2011, 196, 5133.
13. D. Wang, N. Ding, X. H. Song and C. H. Chen, *J. Mater. Sci.*, 2009, **44**, 198.
14. J. Huang and Z. Jiang, *Electrochem. Solid-State Lett.*, 2008, **11**, A116.
15. K. Song, D. H. Seo, M. R. Jo, Y. I. Kim, K. Kang and Y. M. Kang, *J. Phys. Chem. Lett.*, 2014, **5**, 1368.
16. Y. J. Hao, Q. Y. Lai, Y. D. Chen, J. Z. Lua and X. Y. Ji, *J. Alloys Compd.*, 2008, **462**, 404.
17. M. Zhen, X. Guo, G. Gao, Z. Zhou and L. Liu, *Chem. Commun.*, 2014, **50**, 11915.
18. Y. J. Bai, C. Gong, Y. X. Qi, N. Lun and J. Feng, *J. Mater. Chem.*, 2012, **22**, 19054.
19. M. M. Rahman, J. Z. Wang, M. F. Hassan, S. Chou, D. Wexler and H.-K. Liu, *J. Power Sources*, 2010, **195**, 4297.
20. M. M. Rahman, J. Z. Wang, M. F. Hassan, S. Chou, D. Wexler and H. K. Liu, *Adv. Energy Mater.*, 2011, **1**, 212.
21. Y. Q. Wang, L. Gu, Y. G. Guo, H. Li, X. Q. He, S. Tsukimoto, Y. Ikuhara and L. J. Wan, *J. Am. Chem. Soc.*, 2012, **134**, 7874.
22. M. M. Chen, X. Sun, Z. J. Qiao, Q. Q. Ma and C. Y. Wang, *J. Alloys Compd.*, 2014, **601**, 38.
23. X. Li, C. Lai, C. W. Xiao and X. P. Gao, *Electrochim. Acta*, 2011, **56**, 9152.
24. F. Wu, X. Li, Z. Wang and H. Guo, *Nanoscale*, 2013, **5**, 6936.
25. K. M. Kim, K. Y. Kang, S. Kim and Y. G. Lee, *Curr. Appl. Phys.*, 2012, **12**, 1199.
26. J. Wang, H. Zhao, Q. Yang, C. Wang, P. Lv and Q. Xia, *J. Power Sources*, 2013, **222**, 196.
27. J. Sun, D. Teng, Y. Liu, C. Chi, Y. Yu, J. L. Lan and X. Yang, *RSC Adv.*, 2014, **4**, 48632.
28. L. Gao, R. Liu, H. Hu, G. Li and Y. Yu, *Nanotechnology*, 2014, **25**, 175402.
29. W. F. Zhang, Y. L. He, M. S. Zhang, Z. Yin and Q. Chen, *J. Phys. D: Appl. Phys.*, 2000, **33**, 912.
30. Y. F. Tang, F. Q. Huang, W. Zhao, Z. Q. Liu and D. Y. Wan, *J. Mater. Chem.*, 2012, **22**, 11257.
31. L. Shen, C. Yuan, H. Luo, X. Zhang, S. Yang and X. Lu, *Nanascale*, 2011, **3**, 572.
32. H. J. Luo, L. F. Shen, K. Rui, H. S. Li and X. G. Zhang, *J. Alloys Compd.*, 2013, **572**, 37.
33. S. P. Kim, A. C.T. van Duin and V. B. Shenoy, *J. Power Sources*, 2011, **196**, 8590.
34. H. Sun, G. Xin, T. Hu, M. Yu, D. Shao, X. Sun and J. Lian, *Nat. Commun.*, 2014, DOI: 10.1038/ncomms5526.
35. T. Wu, F. Tu, S. Liu, S. Zhuang, G. Jin and C. Pan, *J. Mater. Sci.*, 2014, **49**, 1861.
36. Y. Wang, W. Zou, X. Dai, L. Feng, H. Zhang, A. Zhou and J. Li, *Ionics*, 2014, **20**, 1377.
37. G. N. Zhu, C. X. Wang and Y. Y. Xia, *J. Electrochem. Soc.*, 2011, **158**, A102.
38. G. J. Wang, J. Gao, L. J. Fu, N. H. Zhao, Y. P. Wu and T. Takamura, *J. Power Sources*, 2007, **174**, 1109.
39. K. Y. Kang, Y. G. Lee, S. Kim, S. R. Seo, J. C. Kim and K. M. Kim, Mater. *Chem. Phys.*, 2012, **137**, 169.
40. X. P. Gao, Y. Lan, H. Y. Zhu, J. W. Liu, Y. P. Ge, F. Wu and D. Y. Song, Electrochem. *Solid-State Lett.*, 2005, **8**, A26.
41. Z. W. Zhao, Z. P. Guo, D. Wexler, Z. F. Ma, X. Wu and H. K. Liu, *Electrochem. Commun.*, 2007, **9**, 697.
42. H. Ge, N. Li, D. Li, C. Dai and D. Wang, *Electrochem. Commun.*, 2008, **10**, 719.
43. P. Kubiak, M. Pfanzelt, J. Geserick, U. Hörmann, N. Hüsing, U. Kaiser and M.Wohlfahrt-Mehrens, *J. Power Sources*, 2009, **194**, 1099.
44. E. Baudrin, S. Cassaignon, M. Koelsch, J.-P. Jolivet, L. Dupont and J. M. Tarascon, *Electrochem. Commun.*, 2007, **9**, 337.
45. C. Lai, Y. Y. Dou, X. Li and X. P. Gao, *J. Power Sources*, 2010, **195**, 3676.
46. J. Wang, X. M. Liu, H. Yang and X. D. Shen, *J. Alloys Compd.*, 2011, **509**, 712.